Title: Microstructural and spectroscopic investigations into the effect of CeO_2 additions on the performance of MnO_2 aqueous rechargeable battery

Authors: Manickam Minakshi, David R.G. Mitchell, Melody L. Carter, Dominique Appadoo, Kalaiselvi Nallathamby

PII: S0013-4686(08)01429-1
DOI: doi:10.1016/j.electacta.2008.12.029
Reference: EA 14236

To appear in: *Electrochimica Acta*

Received date: 13-11-2008
Revised date: 18-12-2008
Accepted date: 18-12-2008

Please cite this article as: M. Minakshi, D.R.G. Mitchell, M.L. Carter, D. Appadoo, K. Nallathamby, Microstructural and spectroscopic investigations into the effect of CeO_2 additions on the performance of MnO_2 aqueous rechargeable battery, *Electrochimica Acta* (2008), doi:10.1016/j.electacta.2008.12.029

Microstructural and spectroscopic investigations into the effect of CeO_2 additions on the performance of MnO_2 aqueous rechargeable battery

Manickam Minakshi*, David R. G. Mitchell[1], Melody L. Carter[1], Dominique Appadoo[2] and Kalaiselvi Nallathamby[3]

Faculty of Minerals and Energy, Murdoch University, Murdoch, WA 6150, Australia

[1]Materials and Engineering Science, ANSTO, PMB 1, Menai, NSW 2234, Australia

[2]Australian Synchrotron, Blackburn Road, Clayton, VIC 3168, Australia

[3]Central Electrochemical Research Institute, ECPS Division, Karaikudi, Tamilnadu 630006, India

Abstract

The influence of CeO_2 additions on the electrochemical behaviour of the MnO_2 cathode in a Zn-MnO_2 battery using lithium hydroxide (LiOH) as an electrolyte is investigated using microscopy and spectroscopic techniques. The results showed that such additions greatly improve the discharge capacity of the battery (from 155 to 190 mAh/g) but only from the second discharge cycle onwards. Capacity fade with subsequent cycling is also greatly reduced. With an aim to understand the role of CeO_2 on the discharge-charge characteristics of MnO_2 and its mechanism, we have used a range of microscopy, spectroscopy and diffraction-based techniques to study the process. The CeO_2 is not modified by multiple discharge and charged cycles. The CeO_2 may enhance the discharge-charge performance of the battery by raising the oxygen evolution potential during charging but does not take part directly in the redox reaction.

Keywords: Cerium oxide, manganese dioxide, additive, LiOH, TEM, EELS, IR.

* Corresponding author

Tel.: +61-8-9360-6784. Fax: +61-8-9310-1711. E-mail: minakshi@murdoch.edu.au; lithiumbattery@hotmail.com

Introduction

Since its invention in 1865, the manganese dioxide (MnO_2) battery has continuously been improved starting with the earliest zinc-manganese dry battery, then Zn-MnO_2 primary battery and culminating with the current commercially available alkaline Zinc-MnO_2 battery [1]. This battery type is still in high demand in the consumer market because it is mercury-free, provides high rate capability and the cost is significantly lower than for the dominant rechargeable lithium-ion battery [2, 3]. The primary reasons for using MnO_2 as a cathode material are its low cost, low toxicity and high availability compared with competing battery materials such as Co and Ni [4]. Also, from a thermodynamical point of view, MnO_2 is the most stable form of tetravalent Mn [5] to retain oxygen at standard temperature and oxygen pressure, whereas Co and Ni are thermally unstable [6]. Therefore, MnO_2 based cathodes are attractive for energy storage applications ranging from alkaline to lithium battery and even to supercapacitors [7-8].

In the Zn-MnO_2 battery, the good discharge performance of MnO_2 has motivated researchers to make these batteries rechargeable [9-10]. This would lead more sustainable use of available manganese resources. Among the various polymorphs of MnO_2 [11-12], γ-MnO_2 of the type IBA-32 (International Battery Association) is used in our aqueous Zn-MnO_2 system. Recently, we showed that lithium intercalation can occur in a Zn-MnO_2 battery using aqueous LiOH electrolytes [13]. Further to this, in an attempt to improve the overall performance of this aqueous rechargeable cell we have investigated various additives like TiS_2 [14], TiB_2 [15] and Bi_2O_3 [16] made to the MnO_2 cathode. These additives significantly improve the discharge performance of MnO_2 battery by stabilizing the MnO_2 crystal lattice. This enhances the amount of lithium intercalated into the host MnO_2 structure.

In this paper we report on cerium oxide (CeO_2) modified MnO_2 cathodes that offer an improved discharge capacity. Somewhat surprisingly, this improvement is only evident following the first charging cycle. Cerium oxide is one of the most reactive rare earth metal oxides, and is commonly used as a promoter or support in industrial catalytic processes due to its oxygen storage capacity [17-19]. Cerium oxide also has a good electrical conductivity and diffusivity at ambient temperature [20]. To the best of our knowledge, there has been no work performed on CeO_2 additions to MnO_2 for battery applications. Very recently we carried out an electrochemical characterization into the influence of variable wt % of CeO_2 addition [21] and found increasing the additive level beyond 2 wt % causes a decrease in cell capacity on long term cycling. Hence, in this paper, we have confined our results only to 2 wt% addition. The objective of this work is (a) to understand the role of CeO_2 we compare the electrochemical results with those of the previously published pure MnO_2 (no additive) [22] and (b) to examine the electrode reactions of the discharged-charged cathode using transmission electron microscopy (TEM), X-ray diffraction (XRD) and infra-red spectroscopy (IR).

Experimental

The EMD (electrolytic manganese dioxide; γ-MnO_2) type (IBA sample 32) material used in this work was purchased from the Kerr McGee Chemical Corporation. Cerium oxide (CeO_2) was obtained from Aldrich chemical company. For the electrochemical test, a pellet was prepared by mixing 73 wt % MnO_2 consisting of 2 wt % CeO_2 with 20 wt % acetylene black (A-99, Asbury, USA) and 5 wt % poly (vinylidene difluoride) (PVDF, Sigma Aldrich) binder in a mortar and pestle. An electrochemical cell was constructed with the disk-like pellet as the cathode, Zn metal

as the anode and filter paper as the separator. The electrolyte was a saturated solution of lithium hydroxide (LiOH) containing 1 mol.L^{-1} zinc sulphate ($ZnSO_4$) with a pH equivalent to 10.5. The cell design and its experimental details were similar to those reported earlier [13].

The morphology and interplanar spacings of the products formed before and after discharge were characterized by transmission electron microscopy (TEM), high-resolution TEM (HRTEM) and electron energy loss spectroscopy (EELS) using a JEOL 2010F TEM model operated at 200kV. TEM specimens were prepared by grinding a small fragment scraped from the pressed pellet under methanol and dispersing on a holey carbon support film. Specimens were examined at liquid nitrogen temperature in a cooling stage, to reduce beam damage and contamination effects. For X-ray analysis a Siemens D500 X-ray diffractometer 5635 using Co-Kα radiation was used. The voltage and current were 30 kV and 40 mA. The scan rate was 1 degree per minute. Two theta values were recorded between 20 and 60 degrees. For infrared (IR) analysis, powdered MnO_2 samples were mixed with KBr (potassium bromide) and pressed into disk shaped pellets. These pellets were then mounted on a sample holder and analyses were carried out under vacuum (for an improved performance in mid infrared absorbing H_2O and CO_2) on IFS 125 HR spectrometer (at Australian Synchrotron) using globar as the internal source with 4mm of aperture in the mid infrared region between 650 and 1500 cm^{-1}. The IR absorption spectra were obtained by taking the ratio of the sample spectra to a background (KBr) spectra. The data acquisition was made on OPUS NT software.

Results and Discussion

The multiple galvanostatic discharge-charge curves of 2 wt% cerium oxide/MnO_2 cathode with zinc as anode are shown in figure 1. The cell was discharged and charged at a constant current density of 0.5 mA. cm^{-2} with lower and upper cut-off voltages of 1.0 and 1.9 respectively. The first discharge capacity of the CeO_2 modified cell was 155 mAh/g while 148 mAh/g [14] was obtained from the unmodified cell (no additives). This shows that the effect of cerium oxide on the first discharge cycle is negligible. However, on the second discharge cycle of the CeO_2 modified cell, the utilization of the material was 18% higher with the capacity increased to 190 mAh/g. After multiple discharge cycles (5^{th} cycle) the discharge capacity of this cell was still higher (183 mAh/g) than the unmodified cell. Figure 2 compares the cyclabilities of the CeO_2 modified and unmodified cell. The CeO_2 addition improved the cell discharge capacity but only from the second cycle. The role of cerium oxide as an additive was initially unclear because if it takes part in the reduction/oxidation processes then the first discharge capacity should be higher but that is not observed in Figs. 1 and 2. Hence, in order to elucidate the role of CeO_2 the nature of the cathode material before and after discharge and charge was characterised.

The TEM image of the CeO_2 modified MnO_2 before discharge is shown in Fig. 3. The bright field image showed the MnO_2 to be crystalline and defective. The selected area diffraction (SADP) on this area (Fig. 3a inset) showed the lowest index MnO_2 reflections to be quite diffuse, supporting this. The measured d-spacings were in good agreement with those of reported for MnO_2 ramsdellite structure [23]. Fig. 3b shows a region of MnO_2 containing CeO_2 particles. These were distinct from the MnO_2 particles in that they were more angular (Fig. 3b) and showed very strong

diffraction and kikuchi line contrast, due to the higher mean atomic number and less defective crystal structure respectively. Selected area diffraction of the CeO_2 particles (not shown) yielded spacings consistent with the CeO_2 phase [24]. The CeO_2 particles were typically quite coarse being 100-500nm in diameter. Electron energy loss spectroscopy (EELS) of the MnO_2 phase yielded a mean branching ratio of 0.678 ± 0.005 suggesting the valence state of the Mn in MnO_2 is + 4 [14]. The CeO_2 particles produced consistent EELS spectra, an example of which is shown in Fig. 4a. The CeO_2 EELS spectra showed an intense $M_{4,5}$ doublet at around 900eV. Each of these peaks is further split into a high energy shoulder. The spectra obtained here are very similar to that reported for CeO_2 in the EELS Atlas for CeO_2 [25]. Bright field imaging (Fig. 5a) of the CeO_2 modified material after the first discharge cycle showed the presence of spherical carbon (from acetylene black) and angular MnO_2 particles. Some organic regions were rich in fluorine from the PVDF as binder. Phase identification was confirmed with x-ray microanalysis – not shown. The corresponding diffraction pattern (Fig. 5a inset) shows streaking indicating lamellar structures with short range order. The dark field image of the MnO_2 shows the lamellar structure (Fig. 5b) which could be related to MnOOH phase [26]. Bright field imaging (Fig. 5c) showed angular CeO_2 particles were still present and appeared unchanged after the discharge cycle. The particles were 100-500 nm in diameter and were single crystal. Selected area diffraction of the CeO_2 confirmed it was unchanged by the discharge cycle. The EELS analysis of the discharged CeO_2 modified sample also suggested that the CeO_2 particles were unchanged by the discharge process. The characteristic edge shape (Fig. 4b) was identical to that found in the material prior to discharge (Fig. 4a).

The CeO_2 modified MnO_2 particles after the first charge cycle were similar to those in the discharged state (Fig. 5a). Some elongated Zn and O-rich crystals were found (X in Fig. 6a). The MnO_2 was highly defective (Fig. 6b) and selected area diffraction (not shown) yielded spacings consistent with MnO_2. As before, streaking was present. Bright field imaging of the CeO_2 particles (Fig. 7a) showed them to be highly crystalline. Selected area diffraction (Fig. 7b inset) highlighted the differences between the patterns for the two phases. The MnO_2 was poorly crystalline and contained disorder, resulting in diffuse diffraction features. The CeO_2 was highly crystalline and defect-free resulting in very sharp diffraction rings. The CeO_2 EELS spectra (not shown) was identical to those shown in Figs. 4a and b (before and after discharge respectively) showing the CeO_2 to be unchanged by the electrochemical cycling. Even after many cycles, EELS spectra for the CeO_2, were identical to those of discharged and charged samples, showing that the CeO_2 was not modified by the electrochemical cycling. Although the CeO_2 was unchanged an increase in the first charge capacity of 18% was observed and this increased capacity was retained on subsequent cycling. It is widely know that CeO_2 is an excellent material to release and absorb oxygen reversibly during redox reactions [27]. Hence, this suggests that the cerium oxide may increase the oxygen evolution potential during charging. Oxygen evolution is an unwanted reaction which normally occurs on the positive electrode during charging in the aqueous electrolyte. Suppression of this reaction may therefore encourage more complete conversion of the $LiMnO_2$ phase back to MnO_2 during charging. The effect of CeO_2 was only evident after the first charge cycle, with no influence found during the first discharge cycle. Capacity fading was evident with the pure MnO_2 cathode, but not in the case of the CeO_2 modified material. This suggests that in pure MnO_2 (no additive), a portion of charging process is consumed

by oxygen evolution and upon cycling some of the MnO_2 cathode transforms into less electro-active forms, like manganese oxyhydroxides, limiting the discharge capacity [22]. Capacity fading was not a feature of the CeO_2 modified material. In part this may be due to CeO_2 helping to stabilise the MnO_2 lattice in a manner similar to that described for other additives such as TiS_2, TiB_2 and Bi_2O_3. In addition, the suppression of oxygen evolution reactions may also provide a stronger thermodynamic driving force to transform any of the less electroactive phases which do form, back to the desired MnO_2 phase.

Figs. 8a-c show x-ray diffraction patterns of the CeO_2 modified cathode before and after discharge, and after charging respectively. The before discharge material (Fig. 8a) shows the characteristic peaks of MnO_2 and CeO_2 as quoted in the JCPDS database [23-24]. The discharged cathode (Fig. 8b) shows the emergence of new peaks (*, o, □ and ●). The main Bragg reflection corresponding to graphite (acetylene black) is seen at $2\theta=30°$(C). The original peaks of MnO_2 (+) are replaced by those of a number of new phases whereas the peaks corresponding to CeO_2 are almost unchanged. As indexed in the XRD pattern these new reflections are in good agreement with those reported for the following materials: Mn_2O_3 (*), MnOOH (o), MnO (□) and Li_xMnO_2 (●) i.e. lithium intercalated MnO_2 [23-24, 28]. This shows that during discharge manganese is, in part, reduced to various oxyhydroxides and lithium is also intercalated into the MnO_2 structure to form Li_xMnO_2. The XRD pattern for the charged cathode material (Fig. 8c) was also similar to that of the starting material except a few minor reflections were present identified as being due to Mn_2O_3 and Li_xMnO_2. The CeO_2 peaks were very similar suggesting that ceria is not modified in the electrochemical process. However, peaks corresponding to manganese

oxides and hydroxides and lithium intercalated MnO_2 disappear on charging indicating that the electrochemical process is reversible in the presence of CeO_2.

Infrared spectroscopy has been used to provide further insight into the influence of CeO_2 modified MnO_2 cathode. It is reported that fundamental vibrations of MnO_2 are generated in the far infrared region while those at mid infrared are due to hydrous components of the manganese oxides [29]. The region of interest in this work is the mid infrared, for the samples before and after discharge. These are compared in Figs. 9 a-b. For the discharged sample, new absorption peaks at 1123 and 1432 cm^{-1} are seen. The strong peak at 1123 cm^{-1} demonstrates the existence of γ-OH bonding [30] and the broad peak around 2600 cm^{-1} region (not shown here) is the OH stretching related to the hydrogen bonding [29-31] corresponding to the MnOOH structure. This confirms the behaviour observed through TEM and XRD analysis, namely that manganese oxyhydroxides are formed during discharge. A small vibrational peak at 1432 cm^{-1} in the discharged sample could be related to manganese (II) oxides [29]. The mid infrared spectra of the second charge (Fig. 9c) and second discharge cycle (Fig. 9d) were very similar. In contrast to Figs 9a-b, the absorption peaks at 1123 and 1432 cm^{-1} region were much lower in. These results indicate that manganese oxyhydroxides and oxides are formed only during the first discharge cycle. These unwanted products are shown to be suppressed during charging and further discharging in the presence of CeO_2. This addition clearly enhances the discharge capacity during subsequent cycling.

Conclusions

The electrochemical performance of CeO_2 modified MnO_2 cathode in an aqueous rechargeable battery has been investigated using microscopy and spectroscopic techniques. The CeO_2 additive enhanced the performance of the battery,

increasing the capacity from 155 to 190 mAh/g on the second discharge cycle, representing an increase of 18%. Importantly, this increased capacity was retained on subsequent cycling. As reported in our earlier work, when using pure MnO_2 (no additive) the corresponding cell exhibited a constant capacity fading on subsequent cycling. The influence of CeO_2 may in part arise from a stabilising effect on the MnO_2 crystal lattice during discharge, such as has been found for compounds such as TiB_2 and Bi_2O_3. The CeO_2 may also increase the oxygen evolution potential on the MnO_2 cathode during charging. This results in a greater thermodynamic driving force to transform both lithium intercalated MnO_2 (Li_xMnO_2) along with any less electroactive oxides/hydroxides of Mn back into MnO_2 during charging, thus suppressing the capacity loss.

Acknowledgements

The author (M. M) would like to thank both Australian Nuclear Science and Engineering (AINSE/AINGRA 08048) and Australian Synchrotron (P655) for providing beam time to enable work on TEM and IR facilities.

References

[1] R. K. Ghavami, Z. Rafiei and S.M. Tabatabaei, J. Power Sources 164 (2007) 934-946

[2] C-C Yang and S.-J. Lin, J. Power Sources 112 (2002) 174.

[3] C. M. Julien, Mater. Sci. Eng. R 40 (2003) 47.

[4] N. N. Greenwood and A. Earnshaw, Chemistry of the Elements (first ed.), Pergamon Press, Oxford (1984) pp.1212.

[5] S. Fritsch and A. Navrotsky, J. Am. Ceram. Soc. 79 (1996) 1761.

[6] D. D. MacNeil, Z. Lu, Z. Chen and J. R. Dahn, J. Power Sources 108 (2002) 8.

[7] Y. Kuzoka, C. J. Wen, J. Otomo, M. Ogura, T. Kobayashi, K. Yamada and H. Takahashi, Solid State Ionics 175 (2004) 507.

[8] S. F. Chin, S. C. Pang and M. A. Anderson, J. Electrochem. Soc., 149 (2002) A379.

[9] Y. Shen and K. Kordesch, J. Power Sources 87 (2000) 162.

[10] Y. Sharma, M. Aziz, J. Yusof and K. Kordesch, J. Power Sources 94 (2001) 129-131.

[11] M. M. Thackeray, Prog. Solid State Chem. 25 (1997) 1.

[12] S. Chou, F. Cheng and J. Chen, J. Power Sources 162 (2006) 727.

[13] M. Minakshi, P. Singh, T.B. Issa, S. Thurgate and R. DeMarco, J. Power Sources., 130 (2004) 254.

[14] M. Minakshi, D. R. G. Mitchell and P. Singh, Electrochim. Acta, 52 (2007) 3294.

[15] M. Minakshi, D. R. G. Mitchell and K. Prince, Solid State Ionics, 179 (2008) 355.

[16] M. Minakshi and D. R. G. Mitchell, Electrochim. Acta, 53 (2008) 6323.

[17] C. Tang, Y. Bando, B. Liu and D. Golberg, Adv. Mater. 17 (2005) 3005.

[18] G. M. Christie and F.P.F. van Berkel, Solid State Ionics 83 (1996) 17.

[19] R. Si, Y.-W. Zhang, S. –J. Li, B. –X. Lin and C.-H. Yan, J. Phys. Chem. B 108 (2004) 12481.

[20] J. Bai, Z. Xu, Y. Zheng and H. Yin, Mater. Lett., 60 (2006)1287.

[21] M. Minakshi, N. Kalaiselvi and D. R. G. Mitchell, “Unpublished data” (2008).

[22] M. Minakshi, P. Singh and D.R.G. Mitchell, J. Electrochem. Soc., 154 (2007) A109.

[23] JCPDS Card (No. 43-1455).

[24] JCPDS Card (No. 34-0394).

[25] C. C. Ahn and O. L Krivanek (1983), *EELS Atlas*, Gatan Inc., 780 Commonwealth Drive, Warrendale, Pennsylvania 15086.

[26] Y. Zhang, Y. Liu, F. Guo, Y. Hu, X. Liu and Y. Qian, Solid State Commun., 134 (2005) 523.

[27] Lj. Kudakovic and M. Flytzani-Stephanopoulos, Journal of Catalysis 179 (1998) 203.

[28] JCPDS card (No. 44-0143).

[29] R. M. Potter and G. R. Rossman, Amer. Miner. 64 (1979) 1199.

[30] Y.-T. Wu and C.-C. Hu, Electrochem Solid State Lett. 8 (2005)A240.

[31] A. Novak, Struct. Bond. 18 (1974) 177.

Figure Captions

Fig. 1 Discharge-charge profiles of CeO_2 modified MnO_2 cathode with Zinc as an anode. Cycle numbers are indicated in the figure. The striking behavior here is the difference observed from the 1^{st} and subsequent cycle.

Fig. 2 Variation of discharge capacity as a function of cycle number for the CeO_2 modified MnO_2 and un-modified MnO_2 cell. Amount of CeO_2 additions are indicated in the figure.

Fig. 3 TEM image of the CeO_2 modified MnO_2 before discharge (a) bright field image of MnO_2 particles– inset shows its corresponding selected area diffraction (SADP) and (b) bright field image of CeO_2 particles.

Fig. 4 EELS Ce $M_{4,5}$ spectrum for CeO_2 modified MnO_2 (a) before and (b) after discharge.

Fig. 5 TEM image of the CeO_2 modified MnO_2 after discharge (a) bright field image of MnO_2 particles - inset shows its corresponding selected area diffraction (SADP) (b) dark image of the formation of lamellar structure and (c) bright field image of CeO_2 particles.

Fig. 6 TEM image of the CeO_2 modified MnO_2 after charge (a) bright field image showing Zn and O– rich crystals (at X) and (b) defective MnO_2.

Fig. 7 TEM images of the CeO_2 modified MnO_2 after charge. Bright field images of (a) Region rich in CeO_2 particles, (b) region containing MnO_2 and CeO_2 particles – inset showing its selected area diffraction (SADP).

Fig. 8 XRD patterns of CeO_2 modified MnO_2 (a) before discharge (b) discharged and (c) charged samples.

Fig. 9 Mid infrared spectra of CeO_2 modified MnO_2 (a) before discharge (b) discharged (c) charged and (b) subsequent discharged samples.

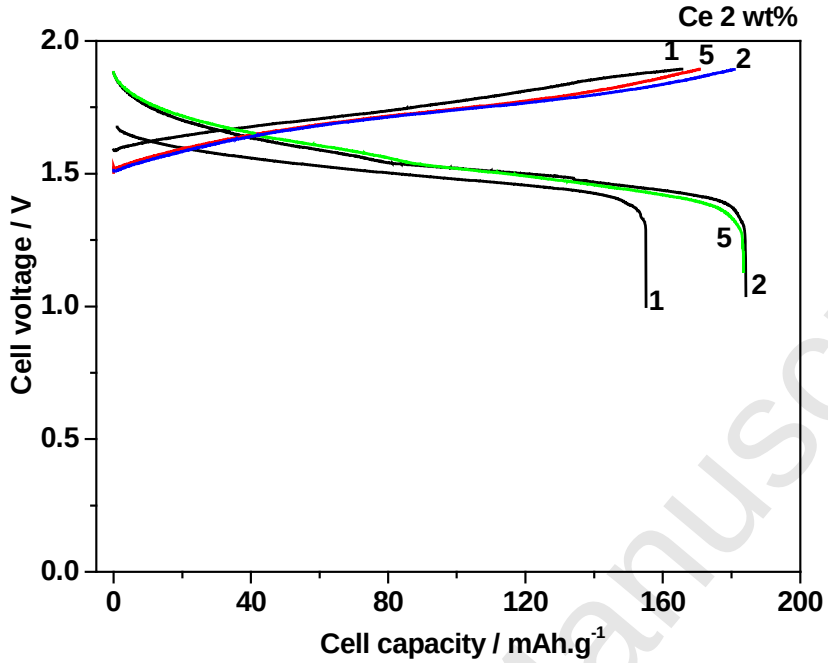

Fig. 1 Discharge-charge profiles of CeO_2 modified MnO_2 cathode with zinc as an anode. Cycle numbers are indicated in the figure. The striking behavior here is the difference observed from the 1st and subsequent cycle.

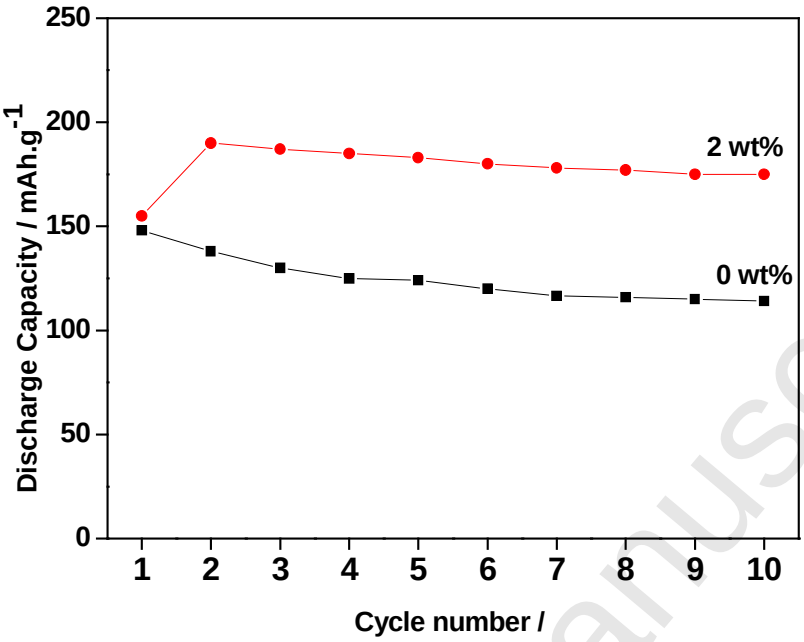

Fig. 2 Variation of discharge capacity as a function of cycle number for the CeO_2 modified MnO_2 and un-modified MnO_2 cell. Amount of CeO_2 additions are indicated in the figure.

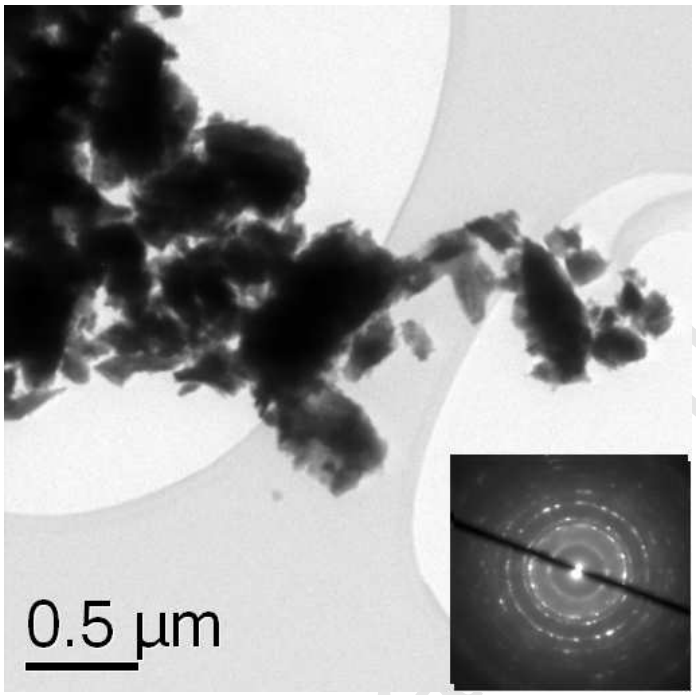

(a)

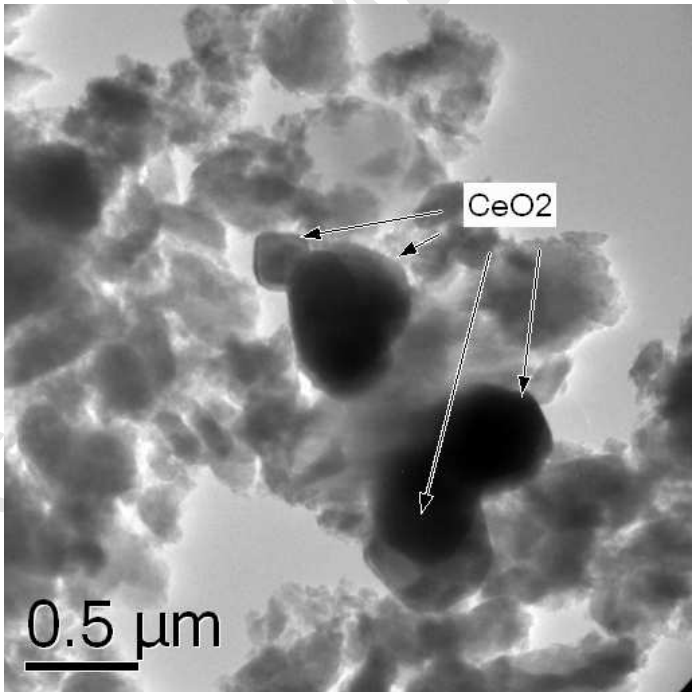

(b)

Fig. 3 TEM image of the CeO_2 modified MnO_2 before discharge (a) bright field image of MnO_2 particles– inset shows its corresponding selected area diffraction (SADP) and (b) bright field image of CeO_2 particles.

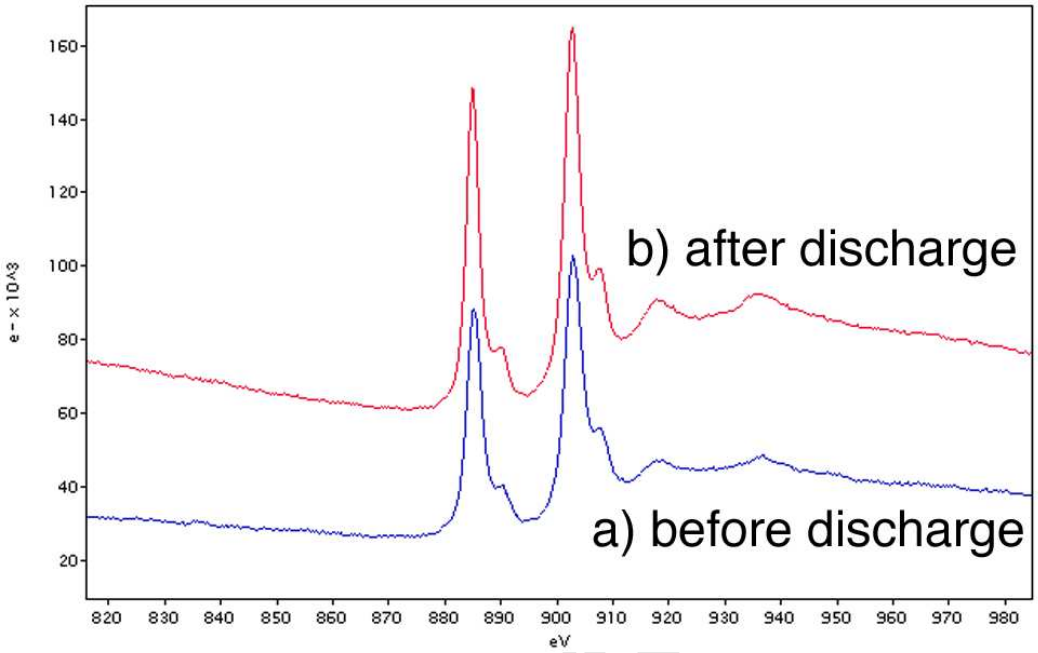

Fig. 4 EELS Ce $M_{4,5}$ spectrum for CeO_2 modified MnO_2 (a) before and (b) after discharge.

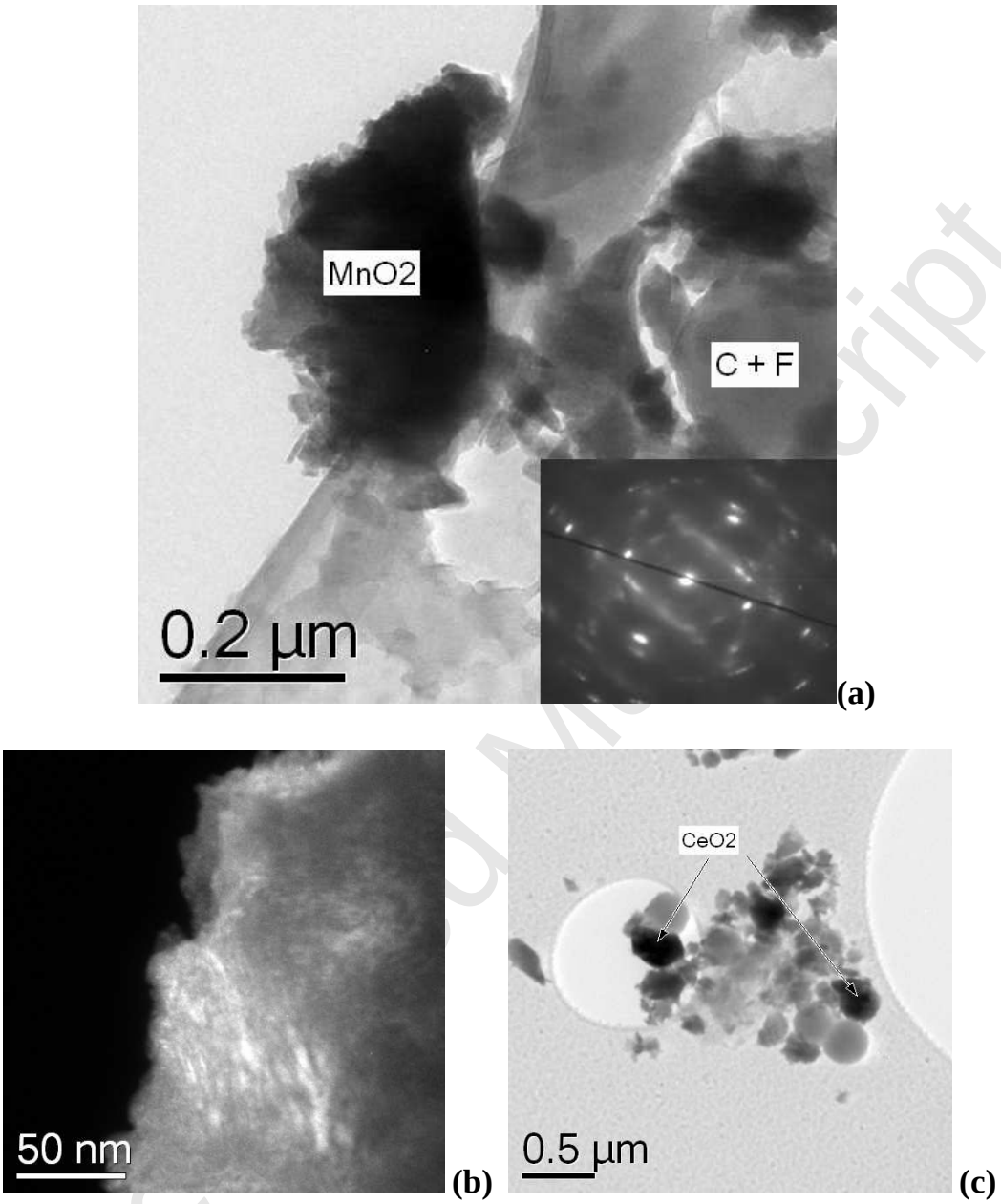

Fig. 5 TEM image of the CeO_2 modified MnO_2 after discharge (a) bright field image of MnO_2 particles - inset shows its corresponding selected area diffraction (SADP) (b) dark image of the formation of lamellar structure and (c) bright field image of CeO_2 particles.

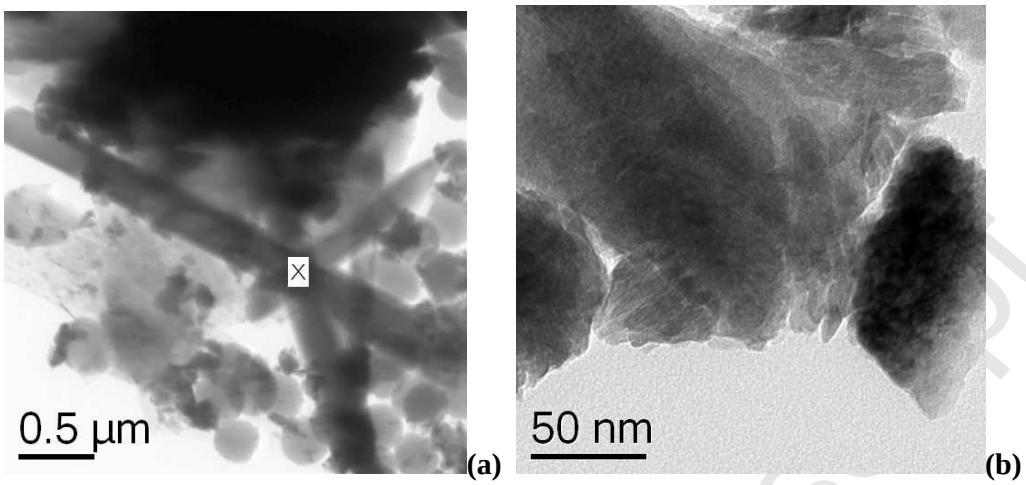

Fig. 6 TEM image of the CeO_2 modified MnO_2 after charge (a) bright field image showing Zn and O– rich crystals (at X) and (b) defective MnO_2.

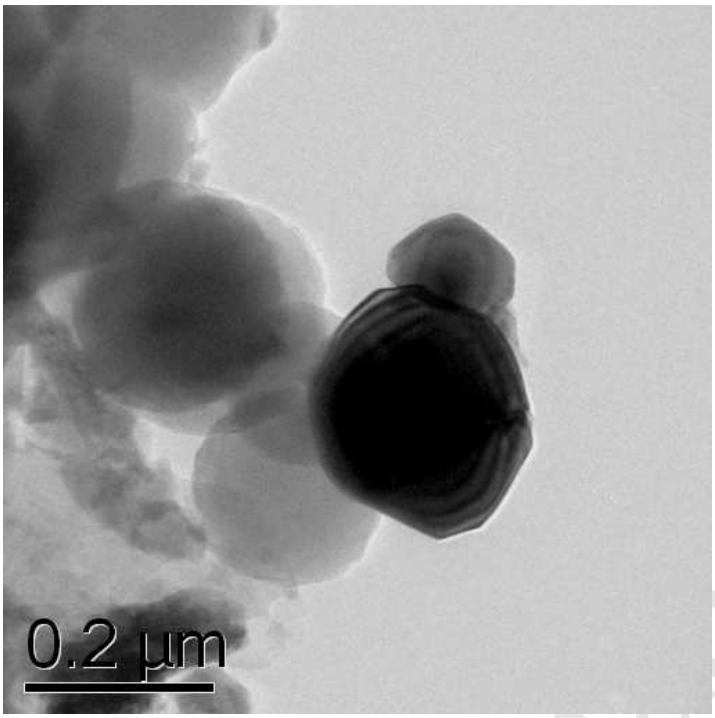

(a)

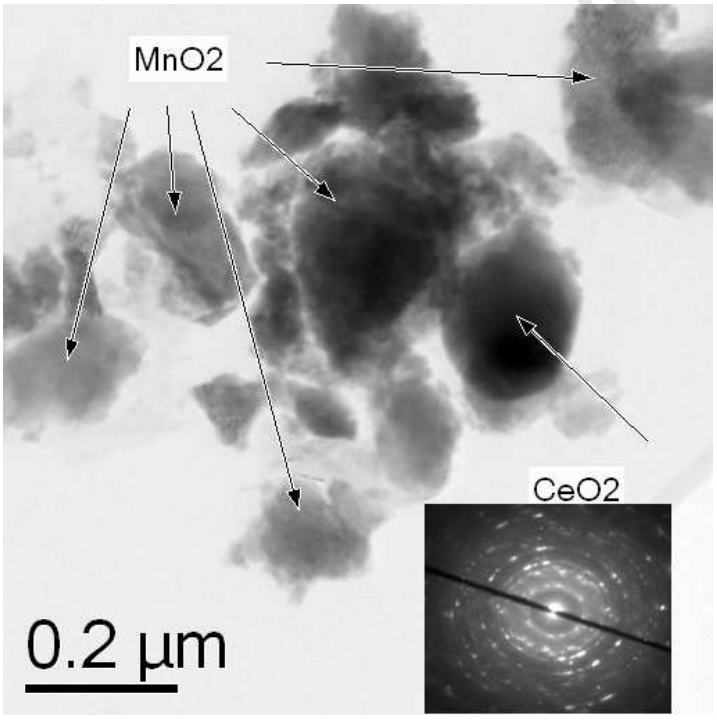

(b)

Fig. 7 TEM images of the CeO_2 modified MnO_2 after charge. Bright field images of (a) Region rich inCeO_2 particles, (b) region containing MnO_2 and CeO_2 particles – inset showing its selected area diffraction (SADP).

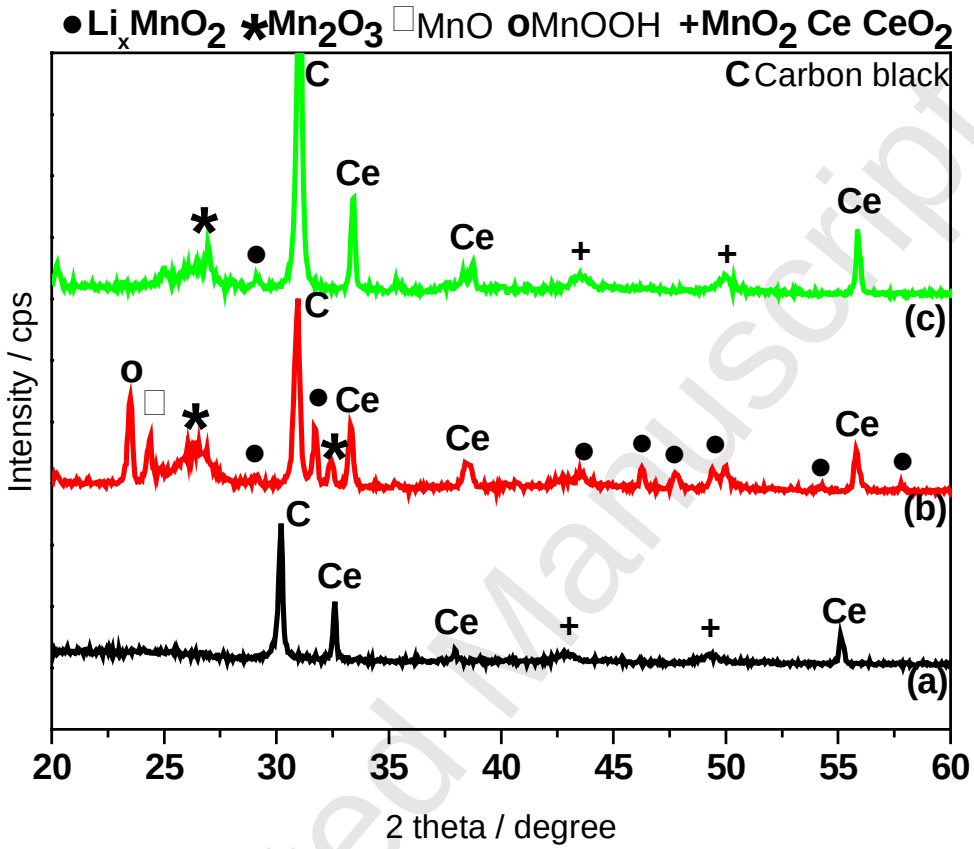

Fig. 8 XRD patterns of CeO_2 modified MnO_2 (a) before discharge (b) discharged and (c) charged samples.

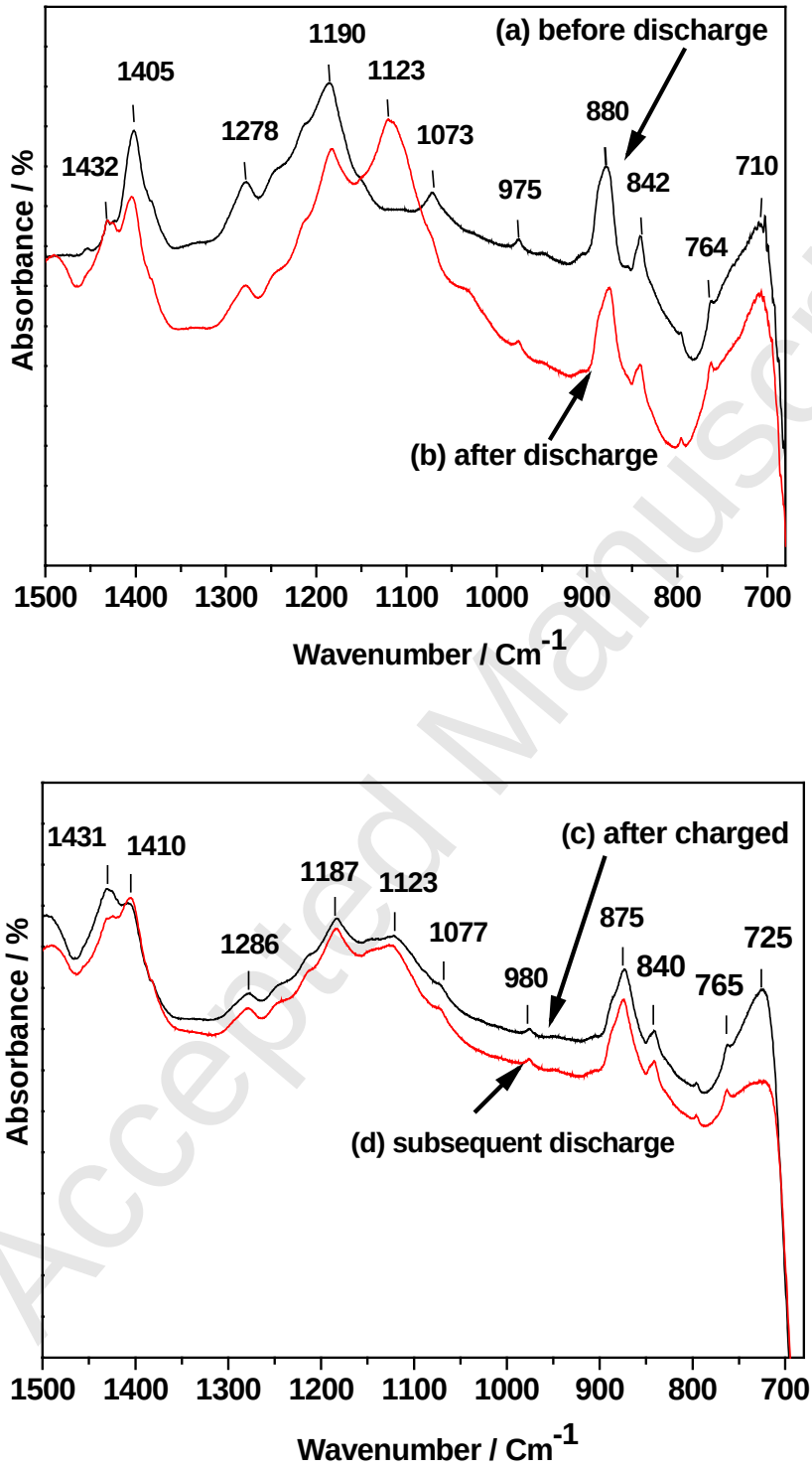

Fig. 9 Mid infrared spectra of CeO_2 modified MnO_2 (a) before discharge (b) discharged (c) charged and (b) subsequent discharged samples.